

20 I. INTRODUCTION

21 Low temperature plasmas play a crucial role in materials processing [1]. Particularly
22 capacitive radio frequency discharges are important. Such plasmas, which were first intro-
23 duced in the 1960s, have undergone a continuous development keeping up with the increasing
24 requirements of the hitech industry. One trend is the attempt to increase productivity by
25 increasing the size of the processed wafers or substrates. In microelectronics, wafer sizes of
26 300 mm are now state of the art, the transition to 450 mm is envisioned [2]. The manu-
27 facturing of flat panel displays or photovoltaic solar cells requires discharges in the meter
28 range [3–5]. The size of the processing equipment obviously must meet these requirements.
29 A second recent trend is the use of higher, often multiple frequencies of up to few hun-
30 dred MHz believed to ensure better power coupling, higher plasma density, and thus higher
31 productivity as well [6, 7].

32 These developments have implications on the physical models which can be used for
33 realistic simulations of plasma-based manufacturing processes. One such implication is of
34 particular importance: The simultaneous increase of driving frequency, plasma density, and
35 discharge size puts the plasmas into a regime where the commonly used “electrostatic ap-
36 proximation” of Maxwell’s equations no longer suffices. That means that $\nabla \times \vec{E} = 0$ (and
37 thus $\vec{E} = -\nabla\Phi$) is not justified anymore. (In this regime the skin depth and/or wavelength
38 of the surface waves propagating in the sheath regions may become comparable or smaller
39 than the reactor dimension). Recent experimental studies have revealed that strong plasma
40 and field non-uniformities appear to be connected with electromagnetic effects [8–13].

41 The theoretical aspects of electromagnetic effects in large-area, high frequency discharges
42 were first systematically studied by Lieberman et al. [14]. They considered an axisymmetric
43 slab model with uniform plasma density in the bulk and the matrix sheath (i.e., constant
44 ion density and zero electron density), treating the plasma as a dielectric and assuming
45 the sheath width to be constant in time. Also, a “natural boundary” condition for a CCP
46 discharge with the dielectric sidewall that all the RF current flows through the discharge
47 (so that the magnetic field at the sidewall is constant in the axial direction and no external
48 source of electromagnetic excitation is involved) was employed. Under these conditions, they
49 treated the problem analytically and gave criteria, based on the estimate of change in the
50 power deposition profile produced by Ohmic heating due to these effects, for significance of

51 the standing wave and skin effects. In essence, a standing wave consists of surface waves,
52 see, e.g., [15], excited in the cavities formed in the powered (grounded) sheath, bounded by
53 the electrode, powered (grounded) sheath interface and the sidewall; the surface waves in
54 the grounded and powered regions are weakly coupled with each other through the bulk.
55 The kind of skin effect meant here manifests itself in tendency of the induced electric field
56 in an RF-driven discharge to reduce current at the axis of the discharge and increase it close
57 to the discharge periphery [16], similar to the skin effect in metals conducting RF current
58 (see, e.g., [17]).

59 Several detailed studies were conducted by Chabert et al. [18] who used a self-consistent
60 transmission line model to account for the interaction of RF heating and plasma density. In
61 recent years the number of contributions to the field has multiplied, for a review see, e.g.,
62 Ref. [19].

63 The analytical models mentioned above, being significantly limited by the underlying
64 assumptions, leave many important questions unanswered. Numerical simulations should
65 be used to describe the phenomena in more realistic situations. So far a number of nu-
66 merical studies based on the fluid models have been conducted for the large scale CCP
67 discharges driven at high frequencies [20–24]. All those approaches were based on the full
68 set of Maxwell’s equations, which contains electromagnetic radiation. The underlying equa-
69 tions are hyperbolic and one has to satisfy the Courant criterion on numerical stability
70 provided an explicit algorithm, such as the popular finite-difference time-domain (FDTD)
71 algorithm, is used for their numerical solution. The Courant criterion forces the time step to
72 be small and the overall simulation time very long. One can resort to implicit algorithms for
73 the numerical solution of Maxwell’s equations, however, it must be noted that the existing
74 implicit numerical schemes are rather intricate.

75 In this paper we propose an alternative numerical approach for studying the large scale,
76 high frequency driven capacitively coupled discharges, which is able to describe the electro-
77 magnetic phenomena occurring in such discharges. The approach is based on the Darwin
78 approximation for solving the system of Maxwell’s equations [25]. The Darwin approxima-
79 tion reduces the original system of hyperbolic equations to a set of elliptic equations by
80 neglecting the transversal part of the displacement current in Ampere’s law, which is justi-
81 fied by a scale analysis of the phenomena of interest. Since the resulting elliptic equations
82 do not support electromagnetic radiation in vacuum, the corresponding Courant criterion

83 is removed and the simulation time step can be chosen as in electrostatic simulations. The
84 required numerical scheme is a relatively simple and straightforward modification of the
85 well-established electrostatic algorithms. It is also important that the approach proposed
86 in this article avoids the computationally expensive iterative schemes used in the previous
87 implementations of the Darwin approximation-based algorithms (see Refs. [26–29]).

88 We demonstrate that the Darwin approximation is in very good agreement with the fully
89 electromagnetic linear treatment of the problem described in [14]. However, realistic plasma
90 density profiles are far from the model used in the latter work, hence next we study the
91 standing wave and skin effect phenomena employing a nonlinear fluid model based on the
92 Darwin approximation with more realistic plasma profiles treated in time domain. Unlike
93 some works (see, e.g., Ref. [22]), which consider excitation of the electromagnetic fields
94 in the discharge coming from external sources, we assume the “natural” excitation of the
95 electromagnetic fields in the CCP discharge generated by the voltage/current that drives the
96 discharge. Obviously, such kind of excitation is always present in the discharge. Also, our
97 Darwin-fluid model accounts for finite electron inertia effects which is necessary in plasmas
98 with low collisions driven at high frequencies.

99 The paper is organized as follows: In Section II we briefly describe the assumptions of
100 the Darwin approximation and its applicability. In Section III we describe the choice of
101 representation for the electromagnetic fields that is particularly convenient for the numeri-
102 cal implementation and a model geometry used in the examples studied in this paper, the
103 boundary conditions are also given in this section. In Section IV we use a linear fluid model
104 solving for the electromagnetic fields in frequency domain both with the Darwin approxi-
105 mation and the full system of Maxwell’s equations for two example cases with pronounced
106 standing wave and skin effects, respectively, to corroborate that the Darwin approximation
107 gives an accurate description of the phenomena in question for the parameters of interest.
108 In Section IV we describe a nonlinear fluid model accounting for the finite electron inertia
109 effects and also using the Darwin approximation to solve for the electromagnetic fields. We
110 demonstrate in a model simulation the standing wave effect for a case with more realis-
111 tic plasma density profiles and sheath dynamics than in cases investigated in Section IV.
112 Finally, we summarize the main results of our study in Section VI.

113 **II. THE DARWIN APPROXIMATION OF THE BOLTZMANN-MAXWELL SYS-**
 114 **TEM**

115 In general, the electrodynamic behavior of any high frequency discharge can be described
 116 by the kinetic equation, such as Boltzmann's equation, supplemented with the system of
 117 Maxwell's equations along with appropriate boundary conditions. Reduced fluid models
 118 can be constructed from this general system by taking moments of Boltzmann's equation
 119 and postulating closure relations. The dynamics of the particle distribution function of
 120 charged species s under influence of electromagnetic forces and collisions is determined by
 121 Boltzmann's equation,

$$\frac{\partial f_s}{\partial t} + \vec{v} \cdot \nabla f_s + \frac{Z_s q_s}{m_s} \left(\vec{E} + \vec{v} \times \vec{B} \right) \cdot \nabla_v f_s = \frac{\partial f_s}{\partial t} \Big|_{\text{col}}. \quad (1)$$

122 In turn, the electromagnetic field is described by Maxwell's equations

$$\frac{1}{\mu_0} \nabla \times \vec{B} = \vec{j} + \epsilon_0 \frac{\partial \vec{E}}{\partial t}, \quad (2)$$

$$\epsilon_0 \nabla \times \vec{E} = -\frac{1}{c^2 \mu_0} \frac{\partial \vec{B}}{\partial t} \quad (3)$$

$$\nabla \cdot \vec{B} = 0, \quad (4)$$

$$\epsilon_0 \nabla \cdot \vec{E} = \rho. \quad (5)$$

123 Direct attempts at numerical solution of (1)-(5) usually require very long simulation time.
 124 This is connected to the fact that this system supports electromagnetic waves in vacuum,
 125 which must be resolved in explicit algorithms in order to avoid numerical instabilities. An-
 126 other approach is to use an implicit algorithm for the numerical solution, where unresolved
 127 electromagnetic modes of no interest are damped numerically. However, such algorithms are
 128 cumbersome to implement and often resort to artificial numerical constructions (see, e.g.,
 129 [15]).

130 A conceptually different alternative is to remove the stiffest time scale in electromagnetic
 131 simulation by reduction of the original system of equations using the assumption about the
 132 time and spatial scales of the expected phenomena. Namely, we use the fact that for the far
 133 most CCP discharges of interest the electrode size is small compared to the wavelength of the
 134 electromagnetic wave in vacuum corresponding to the highest frequency driving harmonics.

135 Following the logic of [30], one can recast (2) and (3) into a normalized form where

136 $\epsilon = L/ct$ with L and t the typical spatial and time scale of the problem,

$$\nabla \times \vec{B} = \vec{j} + \epsilon \frac{\partial \vec{E}}{\partial t}, \quad (6)$$

$$\nabla \times \vec{E} = -\epsilon \frac{\partial \vec{B}}{\partial t}. \quad (7)$$

137 To the zeroth order in ϵ (7) yields $\nabla \times \vec{E} = 0$, so that to this order the electric field is purely
 138 longitudinal (irrotational); we will denote this part of the electric field \vec{E}_L . To the same
 139 order the displacement current drops out of (6). To describe the electromagnetic effects one
 140 needs to include the next order in ϵ , whereby

$$\nabla \times \vec{B} = \vec{j} + \epsilon \frac{\partial \vec{E}_L}{\partial t}, \quad (8)$$

$$\nabla \times \vec{E}_T = -\epsilon \frac{\partial \vec{B}}{\partial t}, \quad (9)$$

141 with \vec{E}_T the transversal (solenoidal) part of the electric field, $\nabla \cdot \vec{E}_T = 0$. (8) and (9)
 142 constitute the Darwin approximation.

143 One can see that this model eliminates electromagnetic waves, but keeps an important
 144 part of the physics, namely electromagnetic effects in the relatively low frequency phenomena
 145 (when the corresponding wavelength in vacuum is larger than the system size). Note that
 146 the corresponding frequencies are called (very) high frequencies in the standard terminology
 147 of the CCP discharges. It is important to note that by dropping the transversal part of the
 148 displacement current the continuity equation remains satisfied.

149 The relation of the Darwin model to the full system of Maxwell's equations can also be
 150 illustrated by the cold unmagnetized plasma dispersion relation,

$$c^2 k^2 + \frac{i\omega\omega_{pe}^2}{i\omega + \nu} - \omega^2 = 0. \quad (10)$$

151 Fig. 1 displays the solutions $k = k(\omega)$ of this relation for a typical parameter combination
 152 ($\omega_{pe} = 2\pi \times 1$ GHz, $\nu/\omega_{pe} = 0.01$). Three distinct regimes can be discerned. Slow phenomena
 153 ($\omega \leq \nu$) are governed by the collisional skin effect $k = (1 - i)/\sqrt{2}\sqrt{\omega/\nu}\lambda_{scf}^{-1}$, with $\lambda_{scf} =$
 154 c/ω_{pe} the collisionless skin-depth. In the intermediate frequency range ($\nu \leq \omega \leq \omega_{pe}$),
 155 the collisionless skin effect prevails, $k = i\lambda_{scf}^{-1}$. Finally, for large frequencies ($\omega > \omega_{pe}$) this
 156 dispersion relation describes propagation of the electromagnetic waves having $k = \omega/c$.

157 In contrast, the dispersion relation of the Darwin model is

$$c^2 k^2 + \frac{i\omega\omega_{pe}^2}{i\omega + \nu} = 0. \quad (11)$$

158 The Darwin model then covers the middle ground between the electrostatic approximation
159 and a fully electromagnetic treatment.

160 Historically, Darwin's original derivation [25] was designed to describe a set of charged
161 particles in free space with velocities small compared to the speed of light. He started from
162 the Lagrangian description of the N -body problem with the interaction incorporated via the
163 retarded Lienard-Wichert potentials. A formal expansion in the smallness parameter v/c ,
164 carried up to the second order, resulted in a simplified Lagrangian with instantaneous (not
165 retarded) potentials. In the same expansion order, relativistic corrections to the equations
166 of motion appeared. For a recent analysis of that approach, see [31].

167 **III. PROBLEM SETUP**

168 For the sake of concreteness, we will consider the same problem setup for studying the
 169 standing wave and skin effect phenomena in CCP discharges as was suggested by Lieberman
 170 et al. [14], i.e., a CCP discharge having cylindrical geometry symmetric in the azimuthal
 171 direction bounded by a dielectric sidewall (see Fig. 2).

172 As all the numerical models described in this article will use the same field equations
 173 stemming from the Darwin approximation of Maxwell's equation, we will describe them in
 174 this section. We saw in the previous section that the electric field in the Darwin approxi-
 175 mation is separated into two parts, a longitudinal part, which is curl-free, and a transversal
 176 part, which is divergence-free. Hence, we choose to represent the electric field in the following
 177 way,

$$\vec{E} = -\nabla\phi + \nabla \times \vec{A}_T, \quad (12)$$

178 where the first (second) term expresses the longitudinal (transversal) part of the electric
 179 field. The longitudinal potential ϕ is governed by Poisson's equation,

$$\nabla^2\phi = -\frac{\rho}{\epsilon_0}, \quad (13)$$

180 with ρ the charge density. To find an equation for the transversal vector-potential \vec{A}_T we
 181 first take the curl of Ampere's law in the Darwin approximation, which results in

$$\nabla^2\frac{\partial\vec{B}}{\partial t} = -\mu_0\nabla \times \frac{\partial\vec{j}}{\partial t}, \quad (14)$$

182 where we used (4). Then, one can exploit Faraday's law using the chosen representation for
 183 the transversal field,

$$\nabla \times \nabla \times \vec{A}_T = -\frac{\partial\vec{B}}{\partial t}. \quad (15)$$

184 Following [14], we consider only TM modes with $\vec{E} = \vec{e}_r E_r + \vec{e}_z E_z$ and $\vec{B} = \vec{e}_\theta B_\theta$, and
 185 $\vec{A}_T = \vec{e}_\theta A_{T\theta}$, so that $\nabla \cdot \vec{B} = 0$ and $\nabla \cdot \vec{A}_T = 0$ hold automatically due to the symmetry of
 186 the problem.

187 In all the following models we study the electromagnetic response to the “natural exci-
 188 tation” of a CCP discharge, prescribing a harmonically varying constant magnetic field at
 189 the sidewall, which is in agreement with the previously made assumption that all the RF

190 current, which drives the discharge, flows through it, and no external excitation source is
 191 involved. Correspondingly, boundary conditions for B_θ is $\partial_z B_\theta = 0$ at the electrodes ($z = -l$
 192 and $z = l$), which is needed in order for the tangential electric field to vanish at the elec-
 193 trodes, and reads $B_\theta = \mu_0 I / (2\pi R)$ at the sidewall ($r = R$) (provided no RF current leaves
 194 the discharge through the dielectric sidewall). Boundary conditions for $\partial_t B_\theta$ are obtained
 195 by taking time derivative of the boundary conditions for B_θ . Further, boundary conditions
 196 for $A_{T\theta}$ are $\partial_z A_{T\theta} = 0$ at the electrodes, so that the tangential component of the transversal
 197 electric field vanishes, and $A_{T\theta} = 0$ at the sidewall. The latter boundary condition for the
 198 $A_{T\theta}$ at the sidewall can be obtained as follows. From the condition that the radial compo-
 199 nent of the transversal electric field vanishes at the dielectric sidewall one can deduce that
 200 $\partial_z A_{T\theta} = 0$ at $r = R$. Integrating this equation with respect to z at $r = R$, matching the
 201 boundary conditions for $A_{T\theta}$ at the electrodes and setting the common constant to zero, one
 202 obtains the boundary condition sought.

203 As the boundary conditions for the longitudinal potential will be slightly different in the
 204 two models studied in this work, we will specify the boundary conditions for each particular
 205 model separately.

206 **IV. LINEAR MODEL PROBLEM WITH FIXED SHEATH TREATED IN FRE-**
 207 **QUENCY DOMAIN**

208 In this section we will demonstrate that the Darwin approximation is a valid approach
 209 for investigation of the electromagnetic phenomena in CCPs by comparing the full elec-
 210 tromagnetic solution to solution obtained with the Darwin approximation for the problem
 211 investigated by Lieberman et al. [14]. The model plasma studied there has uniform ion
 212 density and a stepwise density for the electron component, such that electrons have the
 213 same density as ions in the bulk and zero density in the sheath, the sheath boundaries are
 214 considered to be stationary. The plasma is modeled as a dielectric, change of the electric
 215 field in the sheaths due to motion of the bulk electron plasma component is modeled through
 216 the surface charge created at the interfaces between the bulk plasma and the sheath regions.
 217 This approach is valid for small oscillations of the bulk plasma (see [15]), a more general
 218 case of moving sheath boundary is considered in the next section.

219 Then, using the representation of the electric field given in (12) (which holds in a general
 220 case as well), one can obtain the following system of equations,

$$\nabla \times \frac{1}{\epsilon_L} \nabla \times \vec{B} = \frac{i\omega}{c^2} \nabla \times \frac{\epsilon_T}{\epsilon_L} \nabla \times \vec{A}_T \quad (16)$$

$$\nabla \times \nabla \times \vec{A}_T = -i\omega \vec{B} \quad (17)$$

221 provided all quantities are proportional to $e^{i\omega t}$. In (16) and (17), $\epsilon_L = 1$ in the sheath and
 222 $\epsilon_L = 1 - \omega_{pe}^2/\omega(\omega - i\nu)$ in the bulk. This system of equations describes both fully EM case
 223 (if $\epsilon_T = \epsilon_L$) and the Darwin approximation (if $\epsilon_T = 0$ in the sheath and $\epsilon_T = -\omega_{pe}^2/\omega(\omega - i\nu)$
 224 in the bulk; this expression can be easily obtained in the usual way by using the equation
 225 of motion and Ampere's law in the Darwin approximation).

226 Once one obtains \vec{A}_T and \vec{B} from solution of (16) and (17), the transversal electric field
 227 can be obtained from $\vec{E}_T = \nabla \times \vec{A}_T$ and the longitudinal electric field from Ampere's law,
 228 which provides $\vec{E}_L = -ic^2/\omega\epsilon_L \nabla \times \vec{B} - \epsilon_T/\epsilon_L \nabla \times \vec{A}_T$.

229 Results in Figs. 3 and 4 show the power deposition profiles for two selected cases with
 230 similar parameters to the corresponding cases in [14]. In all cases $d = 2$ cm $s = 0.4$ cm,
 231 and $\nu = 10^7$ s⁻¹. The radial profiles shown in Figs. 3 and 4 are normalized values of
 232 $P_{cap} = \int_0^d |E_z|^2 dz$ and $P_{ind} = \int_0^d |E_r|^2 dz$ [14].

233 calculated with the full system of Maxwell's equations and the Darwin approximation.

234 Not only do both models demonstrate same behavior qualitatively, but also quantitative
235 difference lies within a numerical error for the parameters chosen. Consequently, from this
236 moment on we will suppose that the Darwin approximation is a valid approach for description
237 of the standing wave and skin effects.

238 **V. NONLINEAR MODEL PROBLEM WITH MOVING SHEATH TREATED IN**
 239 **TIME DOMAIN**

240 Although the model problem used [14] and in the previous section gives a certain insight
 241 into the standing wave and skin effects, it is still quite far from realistic CCP plasmas. The
 242 assumptions of stationary sheath boundary and stepwise electron density profile are the
 243 main drawbacks of the model. Most of the previous analytical and numerical treatments of
 244 the standing wave and skin effects in the literature also assumed stationary sheath boundary
 245 with the electrostatic sheath model (e.g., [23]), which makes the corresponding numerical
 246 algorithm faster, but strips the model of adequate description of possible nonlinear phe-
 247 nomena. In [24] the authors studied the problem entirely in the time domain, however, the
 248 commonly adopted drift-diffusion approximation also used in that work is clearly not appli-
 249 cable to the usual range of parameters in low-pressure CCP discharges, when the frequency
 250 of electron collisional momentum transfer is smaller than the driving frequency. In partic-
 251 ular, the highly collisional regime studied in [24] renders direct comparison with results of
 252 [14] impossible, as the latter work was made under the low-collisionality ansatz.

253 To fully resolve the nonlinear discharge dynamics we propose another model, where the
 254 sheath boundary is allowed to move, the plasma density profiles have a more realistic shape,
 255 and the effects of finite electron mass are retained, which makes the model capable of more
 256 general treatment of the electromagnetic phenomena under question in low-pressure CCP
 257 discharges than the model considered in the previous section. The electromagnetic fields in
 258 the sheath region are calculated self-consistently with the plasma dynamics and are treated
 259 in the same way as the rest of the electromagnetic fields in the entire discharge. To keep
 260 the model simple yet comprising all the effects of interest, we adopt a fluid description for
 261 the electron plasma component, whereas ions are assumed to be immobile. In this way we
 262 choose to focus on the coupled dynamics of electrons and the electromagnetic fields in the
 263 entire discharge, omitting the issue of discharge sustainment. Analogously, we substitute
 264 the plasma energy balance equation with the assumption of electron isothermality. The
 265 geometry of the model is the same as considered in the previous section.

266 The evolution of electrons is governed by the momentum equation,

$$\frac{\partial \vec{v}_e}{\partial t} + (\vec{v}_e \cdot \nabla) \vec{v}_e = -\frac{T_e}{m_e} \frac{\nabla n_e}{n_e} - \frac{e}{m_e} \left(-\nabla \phi + \nabla \times \vec{A}_T + \vec{v}_e \times \vec{B} \right) - \nu_m \vec{v}_e, \quad (18)$$

267 and the continuity equation,

$$\frac{\partial n_e}{\partial t} = -\nabla \cdot (n_e \vec{v}_e). \quad (19)$$

268 The boundary conditions for (18) is that the radial component of the electron velocity, $v_{e,r}$,
 269 vanishes at the sidewall, which comes from the assumption that all the electrons are reflected
 270 back into the discharge there, and that the axial component of the electron velocity at the
 271 driven (grounded) electrodes is $v_{e,z} = \pm 1/4 \sqrt{8k_B T_e / \pi m_e}$, respectively, which corresponds
 272 to the kinetically limited flux. The boundary conditions for (19) are, in accordance with
 273 the boundary conditions for (18), that the radial flux to the sidewall vanishes, and the
 274 axial flux to the electrodes is kinetically limited, so that $n_e v_{e,z} = \pm n_e / 4 \sqrt{8k_B T_e / \pi m_e}$ at
 275 the driven (grounded) electrodes, respectively. We take the initial ion density profile to be
 276 of the Gaussian form and the initial electron density profile to be of the same form as the
 277 ion density profile. The numerical discharge simulation gradually develops electron-depleted
 278 sheath regions (see Fig.5).

279 The fields are calculated self-consistently with evolution of the electron plasma component
 280 using (13) to (15)). One can distinguish two different sets of boundary conditions depending
 281 on the way the discharge is driven, either with a voltage source or a current source. Whereas
 282 boundary conditions for (15) are same for both cases (see the discussion at the end of section
 283 III), the boundary conditions for (13) and (14) are different for each case.

284 **A. Voltage-driven discharge**

285 In this case the potential at the driven electrode is prescribed, $\phi(z = -l) = V(t)$. This
 286 gives Dirichlet boundary condition at the driven electrode, the boundary conditions at the
 287 sidewall and the grounded electrode being same in both cases (Neumann boundary condition
 288 at the sidewall, $\partial_r \phi = 0$ and at the grounded electrode Dirichlet boundary condition $\phi = 0$.
 289 (See also the discussion in Section III).

290 The time derivative of the total axial current through the discharge, which enters the
 291 sidewall boundary condition for (14), must be calculated under the circumstances by inte-
 292 grating the plasma current density time derivative, $-e \partial_t (n_e v_{e,z})$ using (18) and (19) over the
 293 surface of any discharge cross-section where the plasma current is dominant, for example,
 294 in the midplane.

295 **B. Current-driven discharge**

296 The potential at the driven electrode is calculate in this case from Kirchhoff's law of
 297 current continuity at the driven electrode, where the sum of the electron current and the
 298 displacement current in the sheath must match the current supplied by the source. We
 299 seek solution to ϕ in the form $\phi = (\phi_0 + \tilde{\phi}(t))\Phi_v + \Phi_\rho$, where $\nabla^2\Phi_v = 0$, where ϕ_0 is the
 300 stationary, and $\tilde{\phi}$ the harmonically changing parts of the potential at the driven electrode,
 301 respectively. The boundary conditions are: $\Phi_v = 1$ at the driven electrode, $\Phi_v = 0$ at the
 302 grounded electrode, and $\partial_r\Phi_v = 0$ at the sidewall; Φ_ρ satisfies $\nabla^2\Phi_\rho = -\rho/\epsilon_0$ with boundary
 303 conditions $\Phi_\rho = 0$ at both electrodes, and $\partial_r\Phi_\rho = 0$ at the sidewall. From the current
 304 balance at the driven electrode one has $-2\pi \int_0^R (en_e v_e + \epsilon_0 \partial_t \partial_z \phi) r dr = I(t)$. Substituing the
 305 chosen form for ϕ into this equation, one obtains an equation for the potential at the driven
 306 electrode

$$\frac{\partial \tilde{\phi}}{\partial t} = - \frac{I(t) + 2\pi \int_0^R (en_e v_{e,z} + \epsilon_0 \partial_t \partial_z \Phi_\rho) r dr}{2\pi \epsilon_0 \int_0^R (\partial_z \Phi_v) r dr} \quad (20)$$

307 The boundary condition for (14) at the sidewall is particularly simple in the case of
 308 current-driven discharge, as one can directly use the value of the time derivative of the total
 309 current supplied by the source.

310 Finally, we want to briefly discuss some details of numerical implementation of (13)),
 311 (14), (15), (18), and (19). We use a leapfrog-like scheme to integrate (18) and (19) in time,
 312 for which we use grids staggered in time for velocity and density, the density and field values
 313 being taken at integral time levels and velocity at the half- time levels. Then, the order of
 314 the whole numerical scheme is the following:

- 315 1. (18) is solved treating the nonlinear second term on the left-hand-side semi-implicitly
 316 thereby linearizing this term with respect to the density taken at the new time level.
 317 The velocity on the right hand side is time-centralized by taking the average between
 318 the new and old time levels, so that it is also semi-implicit. It is worth mentioning
 319 that during the stage of the sheath formation an artificial viscosity term is helpful
 320 in getting rid of numerical instabilities arising at the plasma-sheath interface. Once
 321 smooth sheaths are formed, the viscosity term can be switched off.

- 322 2. The density on the right-hand side of (19) is treated semi-implicitly and is time-
323 centralized using the same technique as in the previous procedure.
- 324 3. (13) is solved with the boundary conditions depending on the way the discharge is
325 driven according to the techniques described above.
- 326 4. The source term in (14) should be calculated using the expression $\partial_t \vec{j}_e = -e(\vec{v}_e \partial_t n_e +$
327 $n_e \partial_t \vec{v}_e)$ with $\partial_t \vec{v}_e$ and $\partial_t n_e$ calculated with help of (18) and (19). An attempt at direct
328 evaluation of $\partial_t \vec{j}_e$ will lead to numerical instability because numerical discretization
329 of a time derivative introduces numerical dispersion and finite field propagation time,
330 whereas conceptually the Darwin approximation expects instantaneous field change in
331 the whole domain (see, e.g., [32]). When calculating the source term for (14), it is also
332 useful to write the term $\mu_0 \nabla \times e^2 n_e / m_e \nabla \times \vec{A}_T$ as $-\lambda_{\text{scf}}^2 \partial_t \vec{B} + \mu_0 e^2 n_e / m_e \nabla n_e \times \nabla \times \vec{A}_T$,
333 where $\lambda_{\text{scf}} = c / \omega_{pe}$ is the collisionless skin depth and we used (15). The first term in
334 this expression describes the collisionless skin effect and can be transferred to the left
335 hand side to be treated implicitly for better numerical stability.
- 336 5. Finally, (15) is solved using the boundary conditions discussed in Section III.

337 One can see that because of the chosen representation for the transversal field as $\vec{E}_T = \nabla \times$
338 \vec{A}_T the cumbersome and computationally expensive iterative scheme needed for making sure
339 that the calculated \vec{E}_T is divergence-free used in the previous implementations of the Darwin
340 codes (see, e.g., [26–29]) is avoided. This is because \vec{E}_T calculated by taking the curl of \vec{A}_T
341 guarantees that \vec{E}_T is divergence-free automatically. To account for the electromagnetic
342 effects in 2D geometry of the problem we described, one needs to solve only two additional
343 elliptic equations using the same field solver that is used for solving Poisson’s equation. It is
344 a small price for removing the very expensive Courant criterion connected with propagation
345 of the light wave, though.

346 In Fig. 5 we show the radial profile of relative power deposition due to the Ohmic heat-
347 ing resulting from a voltage-driven discharge simulation showing a significant standing wave
348 effect for a case with relatively low collisionality ($\nu_m = 1 \times 10^7 \text{ s}^{-1}$). Parameters are sim-
349 ilar to the parameters for the case shown on the top part of Fig. 3. The inductive power
350 deposition is negligible and is not shown. The change of radial power deposition profile is
351 more pronounced for the more realistic Gaussian-like axial electron density profile adopted

352 for the simulation in contrast to the stepwise electron density profile taken for the problem
353 in Section IV. For comparison, we also present the radial profile of relative power deposition
354 obtained with a purely electrostatic simulation. As one can see, the electromagnetic compo-
355 nent is an essential part of the standing wave effect for the parameters in question, despite
356 the fact that surface waves propagating in sheath and generating standing waves may also
357 exist in the electrostatic description (see, e.g., [33]).

358 VI. CONCLUSIONS AND OUTLOOK

359 In this paper we have demonstrated that the Darwin approximation is adequate for de-
360 scription of the standing wave and skin effects present in the high frequency CCP discharges
361 by comparing relevant electromagnetic fields calculated using the approximation and solu-
362 tion of the full set of Maxwell's equations for two different typical cases exhibiting such
363 effects in a model problem. We considered the "natural" excitation of such effects coming
364 from the current driving the discharge needed for its very existence. The Darwin approxima-
365 tion reduces originally hyperbolic Maxwell's equations, by dropping the transversal current
366 in Ampere's law, to a set of elliptic equations which do not support light waves propagating
367 in vacuum. This has very significant consequence for the numerical algorithms based on
368 that approach that the corresponding Courant criterion is also removed, enabling same time
369 step size as in electrostatic algorithms. We have shown that the Darwin approximation can
370 be straightforwardly implemented in fluid models, requiring only a slight modification of
371 a possibly existing electrostatic code with the eventual great computational pay-off. The
372 choice of the representation for the transversal field proposed by us helps to avoid the com-
373 putationally demanding iterative schemes needed for its divergence cleaning used in other
374 implementations. Using a reduced nonlinear fluid code self-consistently evolving plasma and
375 electromagnetic fields in time domain, on the example of a case exhibiting standing wave
376 effect we have shown that the electromagnetic effects not only are present but can be even
377 more significant for more realistic profiles and sheath dynamics.

378 The proper description of low-pressure CCP discharges ultimately requires a kinetic tool
379 as kinetic effects are essential in such discharges. The use of the Darwin approximation is,
380 of course, not limited to fluid models. The sheath dynamics, the heating mechanisms other
381 than the Ohmic heating, the nonlocal transport phenomena all demand kinetic treatment.
382 The Darwin numerical algorithm for the solution of the electromagnetic fields designed in
383 this work can be also used in a Particle-in-Cell code. The reduced fluid model developed in
384 this work can, in turn, serve as benchmark for such a code.

385 **ACKNOWLEDGMENTS**

386 The authors gratefully acknowledge the support by the Deutsche Forschungsgemeinschaft
387 via the Sonderforschungsbereich TRR 87.

-
- 388 [1] M. A. Lieberman and A. J. Lichtenberg, *Principles of Plasma Discharges and Materials Pro-*
389 *cessing* (Wiley, New York, 2005), 2nd ed.F
- 390 [2] S. Samukawa, M. Hori, S. Rauf, K. Tachibana, P. Bruggeman, G. Kroesen, J. C. Whitehead,
391 A. B. Murphy, A. F. Gutsol, S. Starikovskaia J. Phys. D: Appl. Phys. **45** , 253001 (2012)
- 392 [3] A. E. Park, B. U. Cho, and J. K. Lee. IEEE Trans. Plasma Sci. **31**, 628, (2003)
- 393 [4] J. Schmitt. M. Elyaakoubi, and L. Sansonnens, Plasma Sources Sci. Technol. **11**, 206 (2002)
- 394 [5] J. Perrin, J. Schmitt, C. Hollenstein, A. Howling, and L. Sansonnens Plasma, Phys. Control.
395 Fusion. **42**, 353 (2000)
- 396 [6] H. H. Goto, H. D. Löwe, and T. Ohmi, J. Vac. Sci. Technol. A **10**, 3048, (1992)
- 397 [7] N. Nakano and T. Makabe, J. Phys. D **28**, 31, (1995)
- 398 [8] L. Sansonnens and J. Schmitt, Appl. Phys. Lett. **82**, 182 (2003)
- 399 [9] A. A. Howling, L. Sansonnes, J. Ballutaud, and C. Hollenstein, J. Appl. Phys **96**. 5429 (2004)
- 400 [10] A. Perret, P. Chabert, J.-P. Booth, J. Jolly, J. Guillon, and P. Auvray, Appl. Phys. Lett. **83**,
401 243 (2003)
- 402 [11] P. Chabert, J.-L. Raimbault, J.-M. Rax, and A. Perret, Phys. Plasmas **11**, 4081 (2004)
- 403 [12] G. A. Hebner, E. V. Barnat, P. A. Miller, A. M. Paterson, and J. P. Holland, Plasma Sources
404 Sci. Technol. **15**, 879 (2006)
- 405 [13] P. A. Miller, E. V. Barnat, G. A. Hebner, A. M. Paterson, and J. P. Holland, Plasma Sources
406 Sci. Technol. **15**, 889 (2006)
- 407 [14] M. A. Lieberman, J.-P. Booth, P. Chabert, J.-M. Rax, and M. M. Turner, Plasma Sources
408 Sci. Technol. **11**, 283 (2002)
- 409 [15] K. J. Bowers, Thesis (PhD), UNIVERSITY OF CALIFORNIA, BERKELEY, Source DAI-B
410 62/07, p. 3254 (2002)
- 411 [16] T. Mussenbrock, T. Hemke, D. Ziegler, R.P. Brinkmann, M. Klick, Plasma Sources Sci. Tech-
412 nol. **17**, 025018 (2008)
- 413 [17] S. Ramo, J. R. Whinnery, and T. Van Duzer, *Fields and Waves in Communication Electronics*,
414 3rd ed., New York, NY: Wiley, 1994
- 415 [18] P. Chabert, J.-L. Raimbault, J.-M. Rax, and M. A. Lieberman, Phys. Plasmas **11**, 1775 (2004)
- 416 [19] P. Chabert, J. Phys. D: Appl. Phys. **40**, R63 (2007)

- 417 [20] Z. Chen, S. Rauf, K. Collins, *J. Appl. Phys.* **108**, 073301 (2010)
- 418 [21] S. Rauf, K. Bera, K. Collins, *2008 Plasma Sources Sci. Technol.* **17** 035003 (2008)
- 419 [22] Y. Yang and M.J. Kushner, *Plasma Sources Sci. Technol.* **19**, 055011 (2010)
- 420 [23] I. Lee, D.B. Graves, and M.A. Lieberman, *Plasma Sources Sci. Technol.* **17** 015018 (2008)
- 421 [24] Y.-R. Zhang, X. Xu, S.-X. Zhao, A. Bogaerts, Y.-N. Wang, *Phys. Plasmas* **17** 113512 (2010)
- 422 [25] C. G. Darwin, *Philos. Mag.*, **39**, no. 233, 537 (1920)
- 423 [26] D. W. Hewett and J. K. Boyd, *J. Comp. Phys.* **70**, 166 (1987)
- 424 [27] D. W. Hewett, *Comp. Phys. Comm.* **84**, 243 (1994)
- 425 [28] M. R. Gibbons and D. W. Hewett, *J. Comp. Phys.* **120**, 231 (1995)
- 426 [29] M. R. Gibbons and D. W. Hewett, *J. Comp. Phys.* **130**, 54 (1997)
- 427 [30] P. A. Raviart and E. Sonnendrücker, *Numer. Math* **73**, 329 (1996)
- 428 [31] T. B. Krause, A. Apte, P. J. Morrison, *Phys. Plasmas* **14**, 102112 (2007)
- 429 [32] C. W. Nielson and H. R. Lewis, *Methods Comput. Phys.* **16**, 367 (1976)
- 430 [33] D. J. Cooperberg, *Phys. Plasmas*, **5**, 853 (1998)

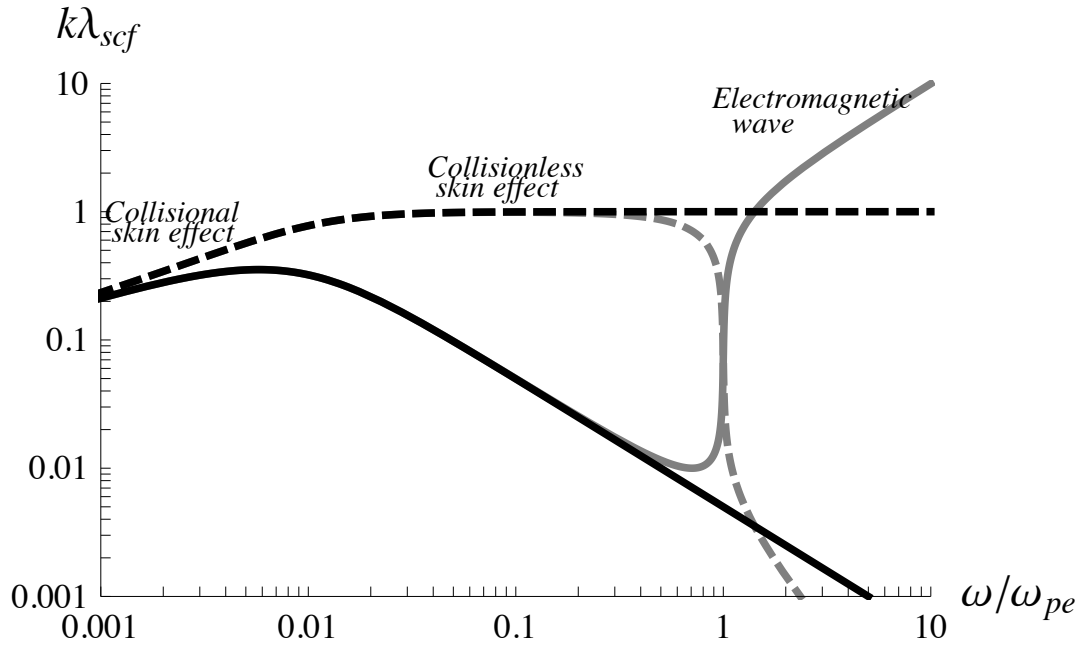


FIG. 1. The dispersion relation obtained with Darwin approximation closely follows the full electromagnetic dispersion relation as long as $\omega < \omega_{pe}$. Solid curves denote the corresponding real and dashed ones imagin

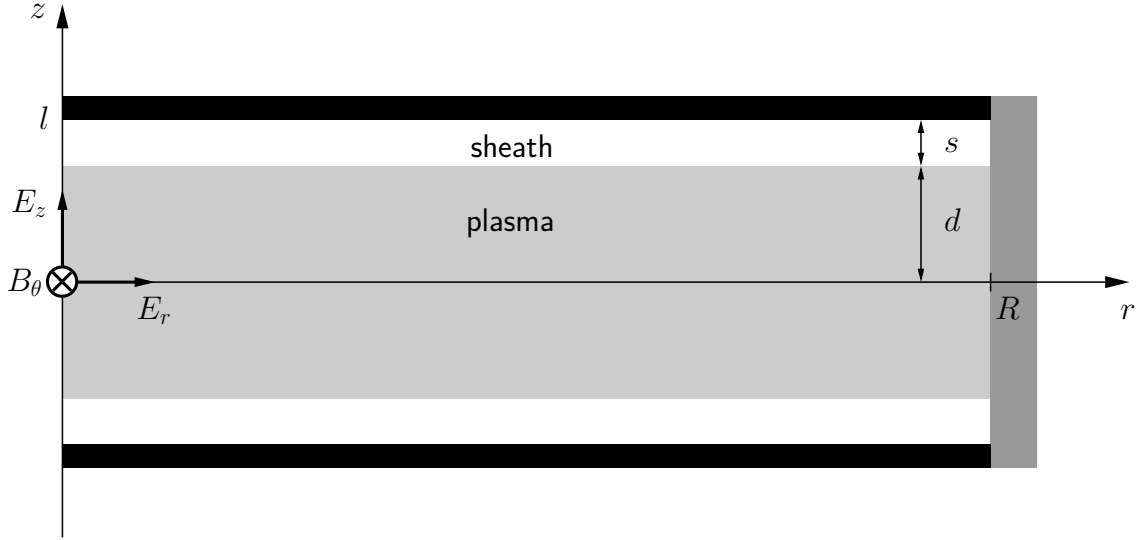


FIG. 2. Sketch of the problem geometry studied in both fluid models. The cylindrical CCP discharge under scrutiny has symmetric electrodes, a sidewall made of dielectric and a plasma. The boundary at the sheath-plasma interface is stationary in the model described in Section IV, whereas in the model of Section V it is allowed to move under the influence of electromagnetic fields. The electromagnetic fields under interest consist of the TM modes in such a plasma-filled cavity and have nonzero E_z, E_r components for the electric, and B_θ component for the magnetic fields, respectively.

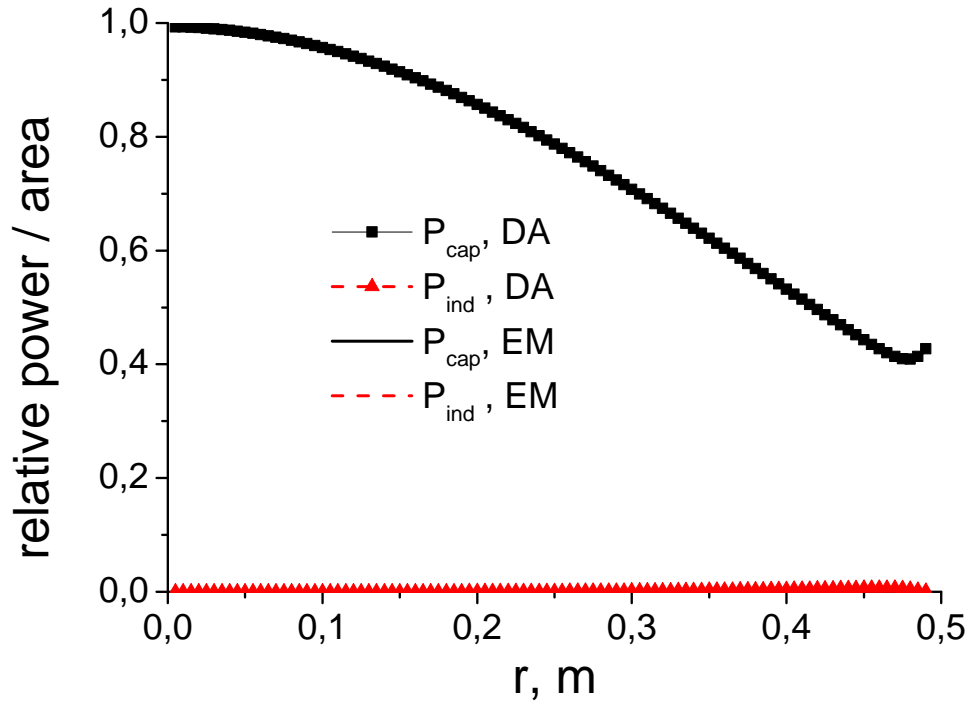


FIG. 3. Comparison of solutions obtained with Darwin approximation (DA) and full system of Maxwell's equations (EM). The first case, which exhibits a strong standing wave effect, has $f = 40,7 \text{ MHz}$ and $n = 10^{15} \text{ m}^{-3}$.

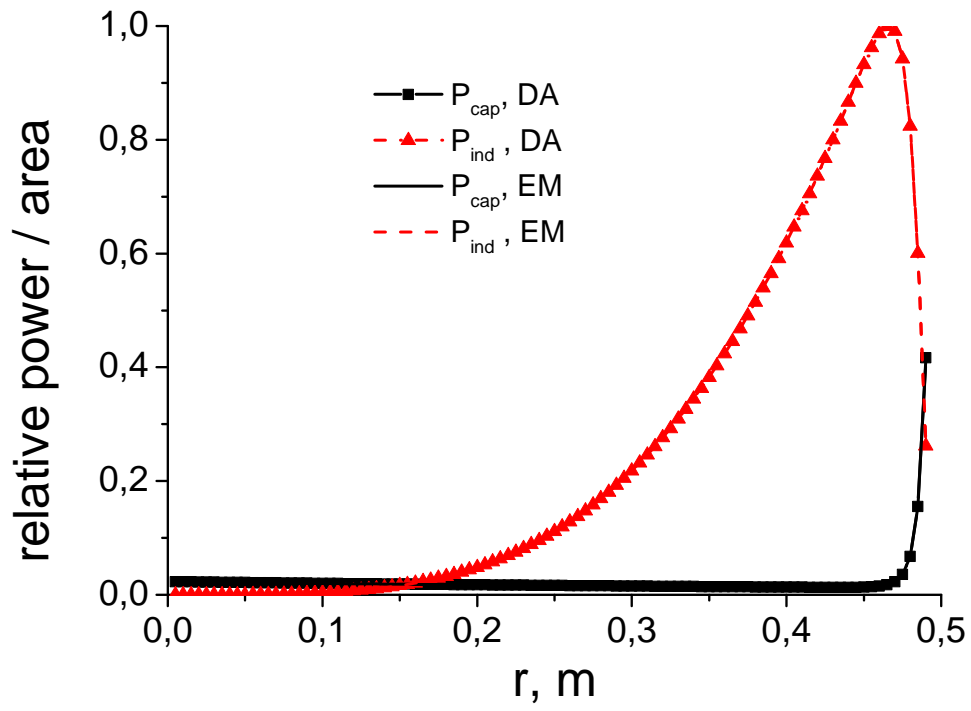


FIG. 4. The second case shows a strong skin effect and has $f = 13.56$ MHz and $n = 10^{17} \text{ m}^{-3}$.

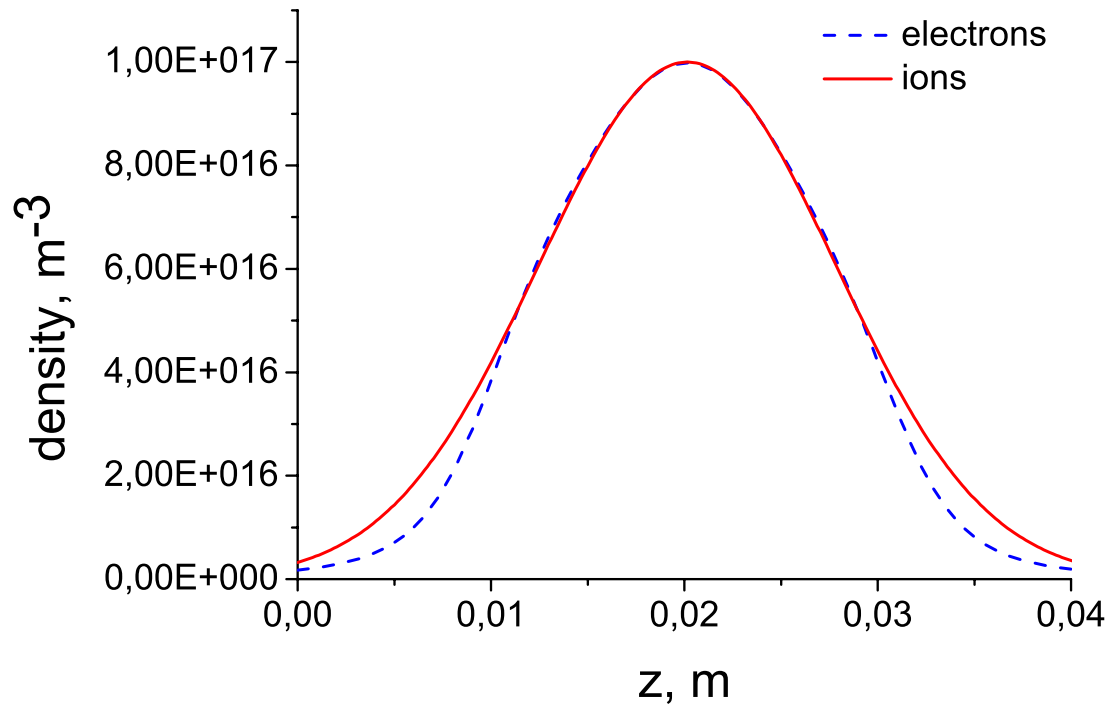


FIG. 5. Development of the sheath regions with depleted electrons in a typical simulation

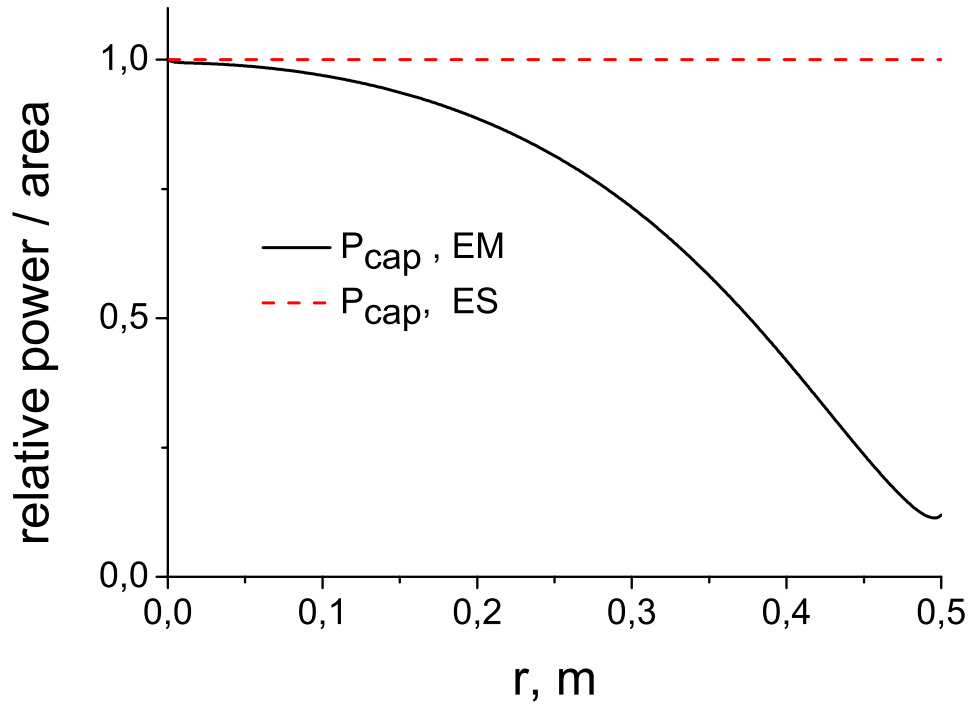


FIG. 6. Relative power deposition radial profile (Ohmic heating) for a case with $f = 40.7$ MHz and $n_{e,max} = 1 \times 10^{15} \text{m}^{-3}$